Azo–hydrazone tautomerism observed from UV–vis spectra by pH control and metal-ion complexation for two heterocyclic Disperse Yellow dyes

Xiao-Chun Chen, Tao Tao, Yin-Ge Wang, Yu-Xin Peng, Wei Huang, Hui-Fen Qian

Electronic Supporting Information

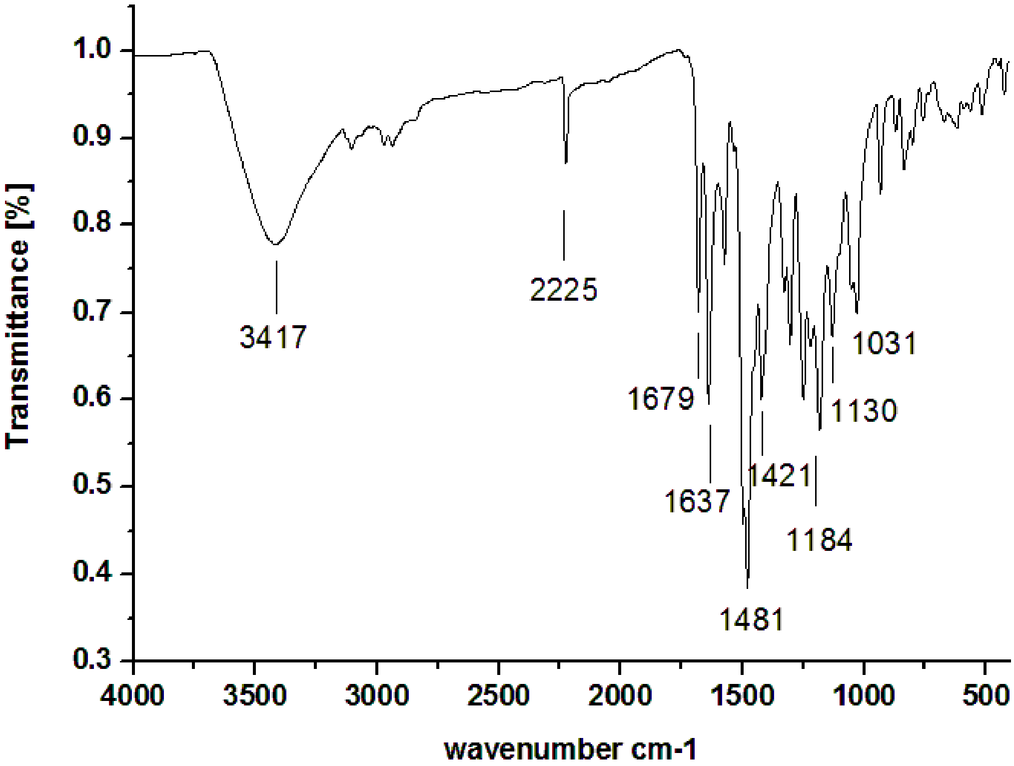

Fig. SI1. FT–IR spectrum of H$\mathbf{L}_{1\text{-}H}$.

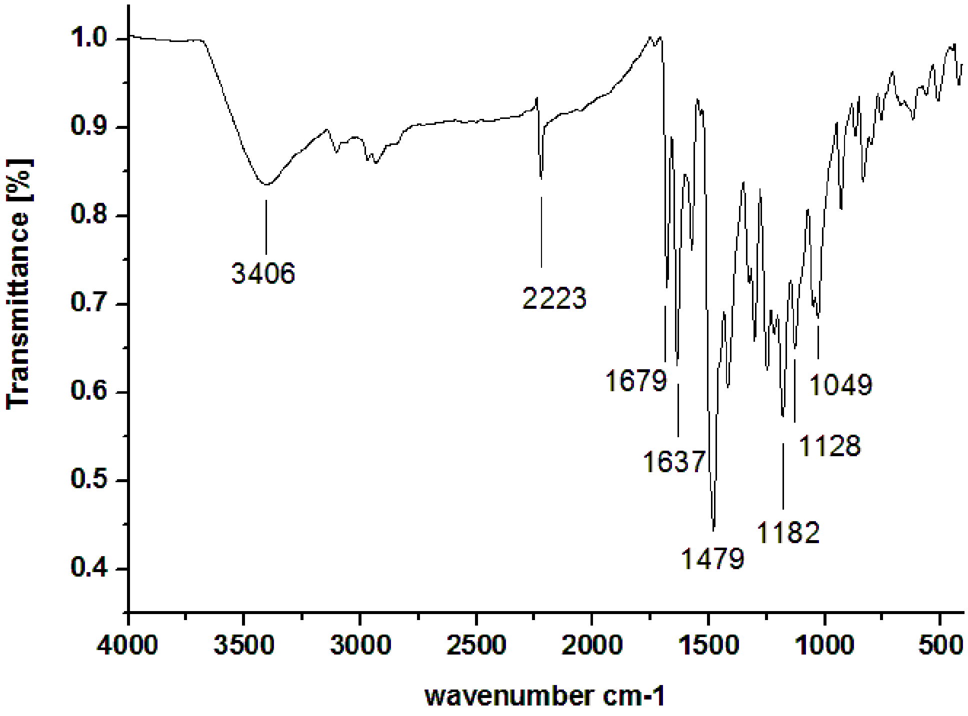

Fig. SI2. FT–IR spectrum of $H\mathbf{L}_{2\text{-}H}$.

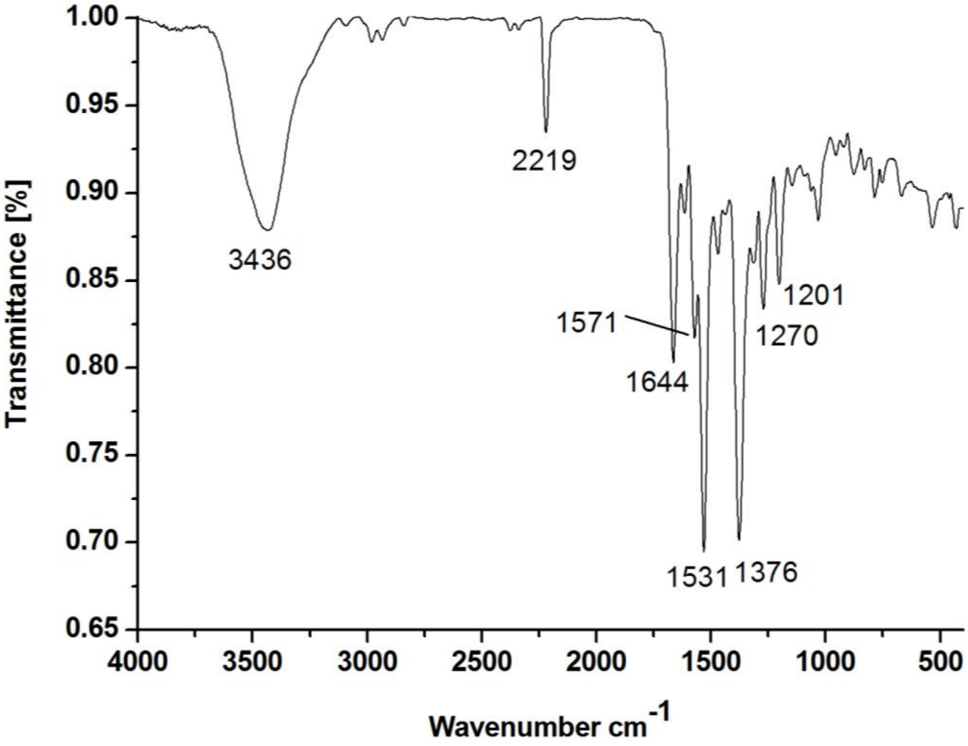

Fig. SI3. FT–IR spectrum of $Cu_2(\mathbf{L}_{2\text{-}A})_4$.

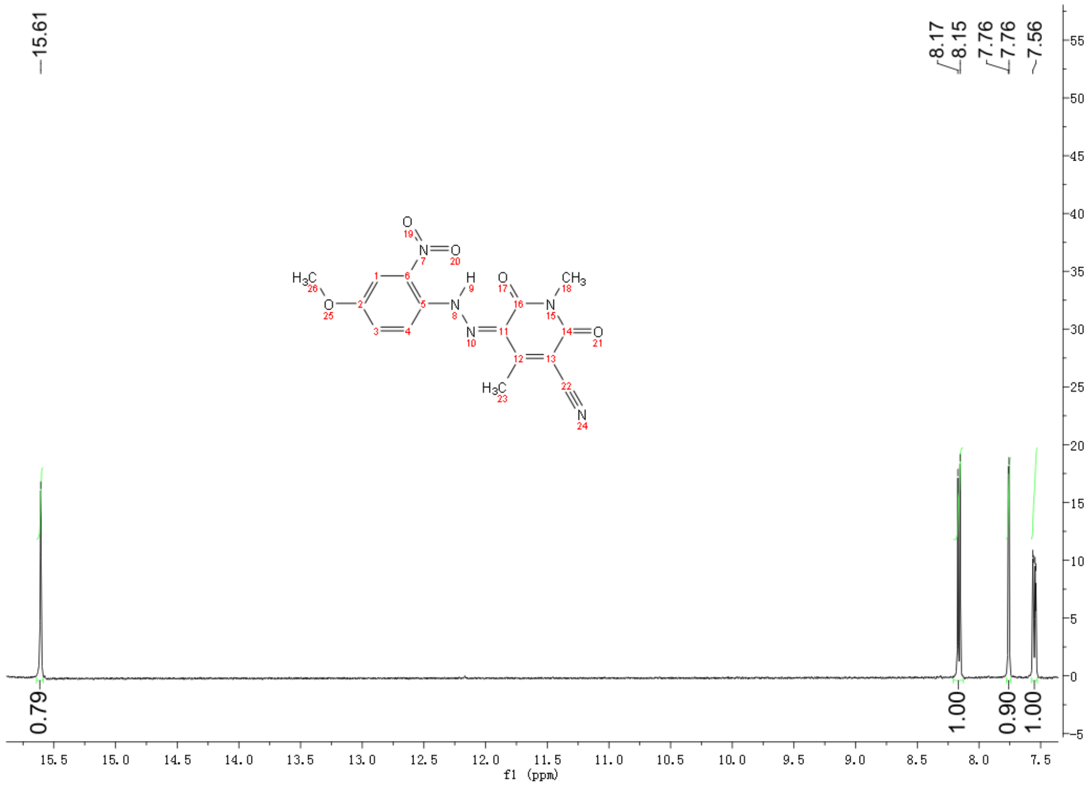

Fig. SI4. ^{1}H NMR spectrum of H$\mathbf{L}_{\mathbf{1\text{-}H}}$ at the low-field range.

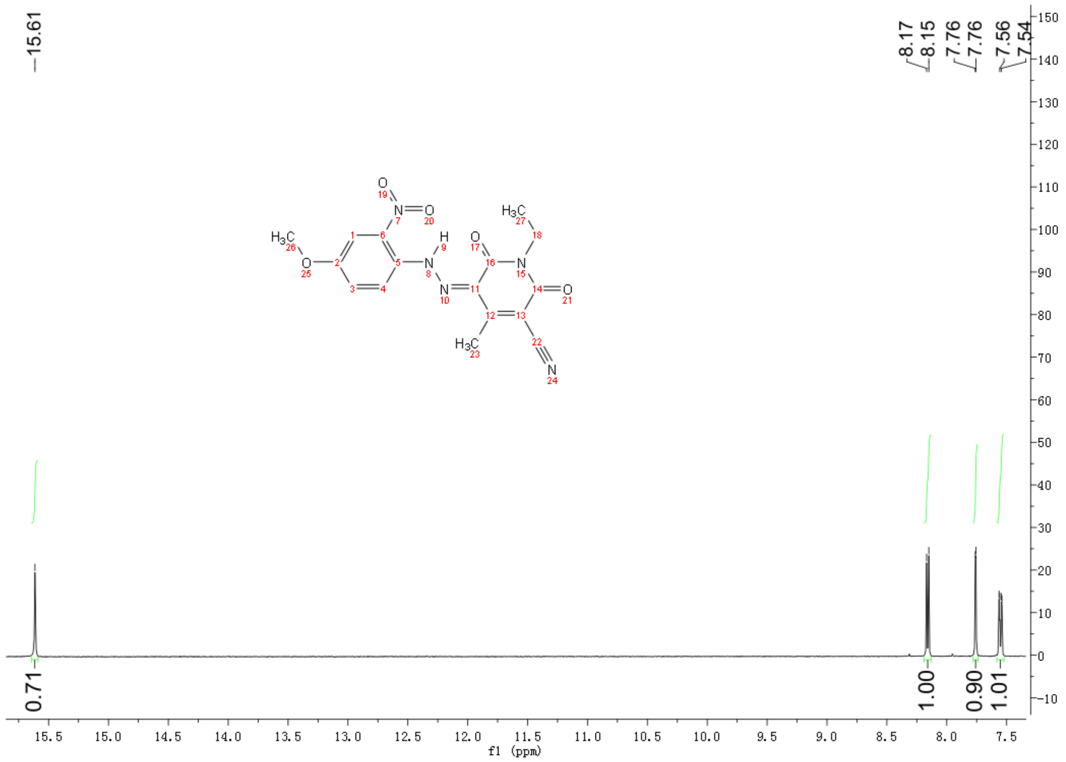

Fig. SI5. ^{1}H NMR spectrum of H$\mathbf{L}_{\mathbf{2\text{-}H}}$ at the low-field range.

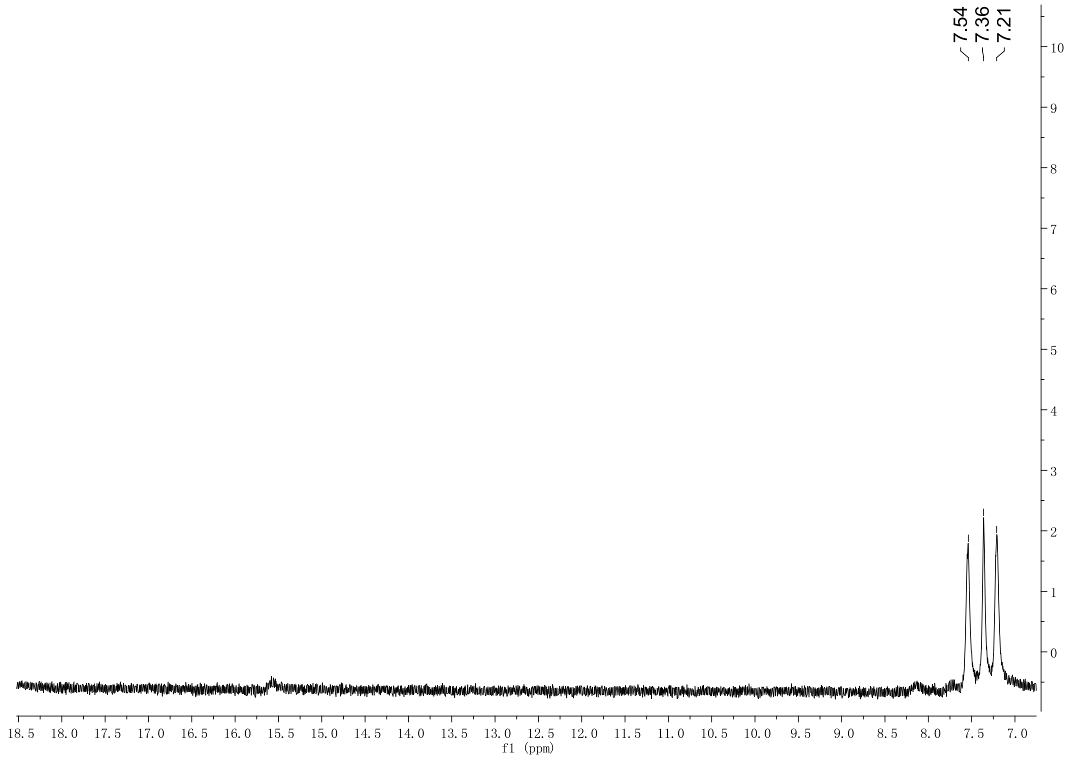

Fig. SI6. ^{1}H NMR spectrum of H$\mathbf{L}_{\mathbf{1\text{-}H}}$ by adding solid NaOH in its DMSO-d^{6} solvent.

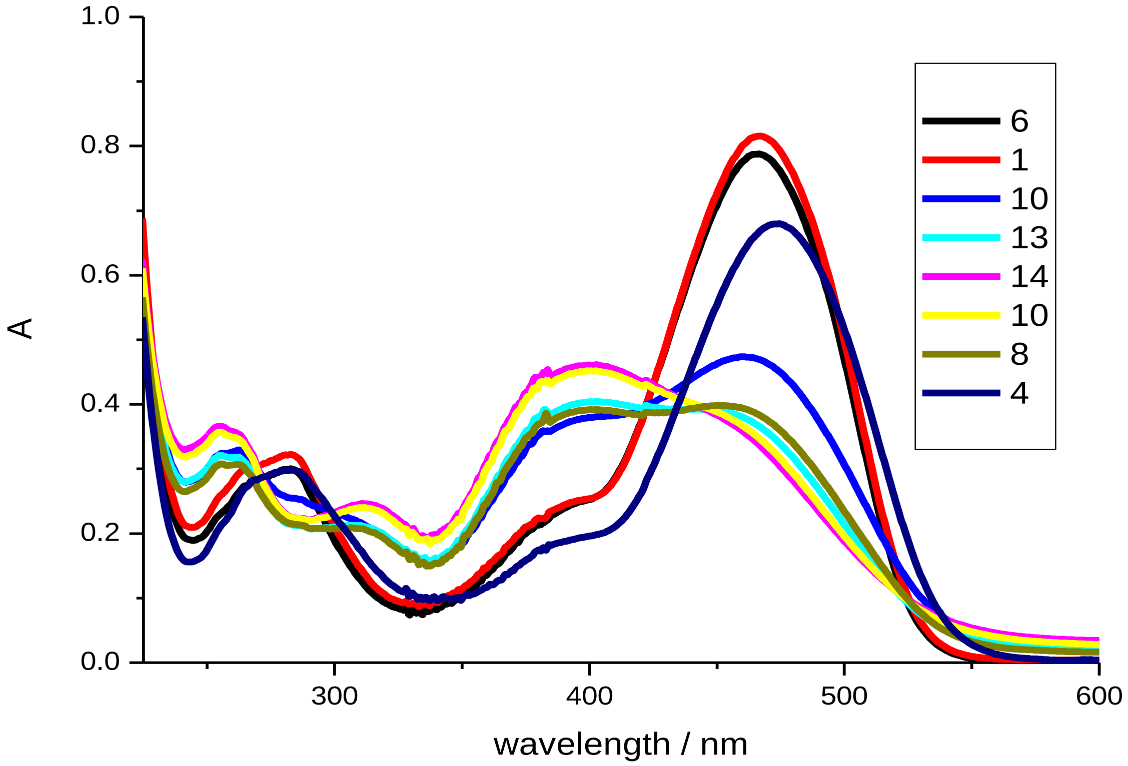

Fig. SI7. UV–vis absorption spectra of dye H$\mathbf{L}_{\mathbf{1\text{-}H}}$ in methanol at room temperature. pH values are adjusted by dropping excess NaOH and then different amounts of HCl.

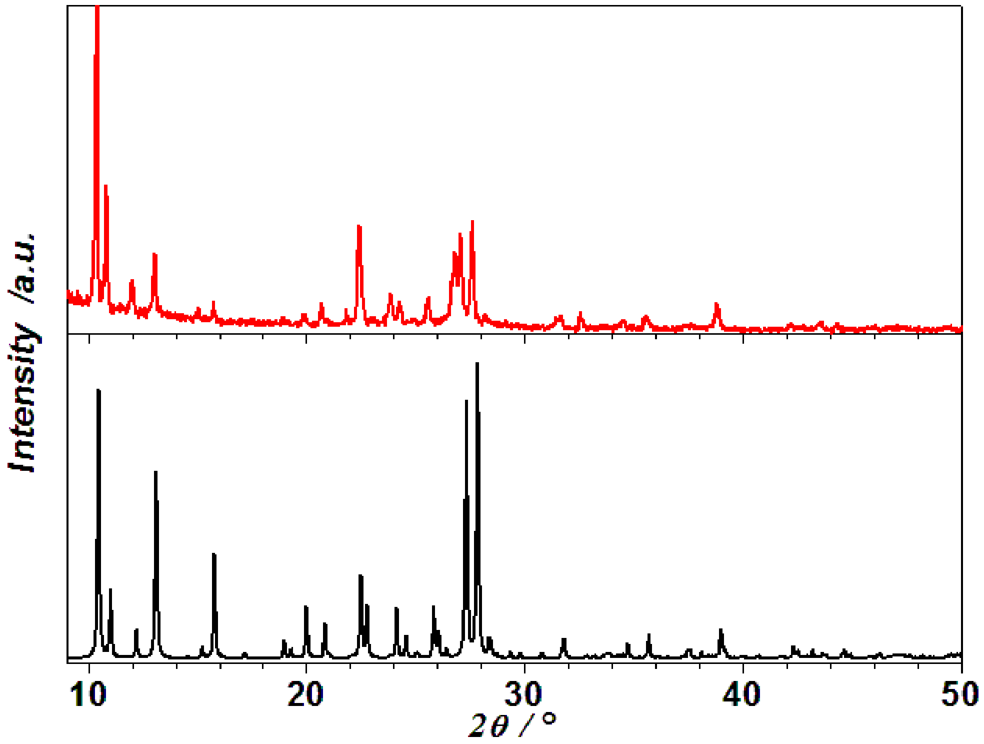

Fig. SI8. The simulative (black line) and experimental (red line) powder X-ray diffraction patterns for H$\mathbf{L}_{\mathbf{1-H}}$.

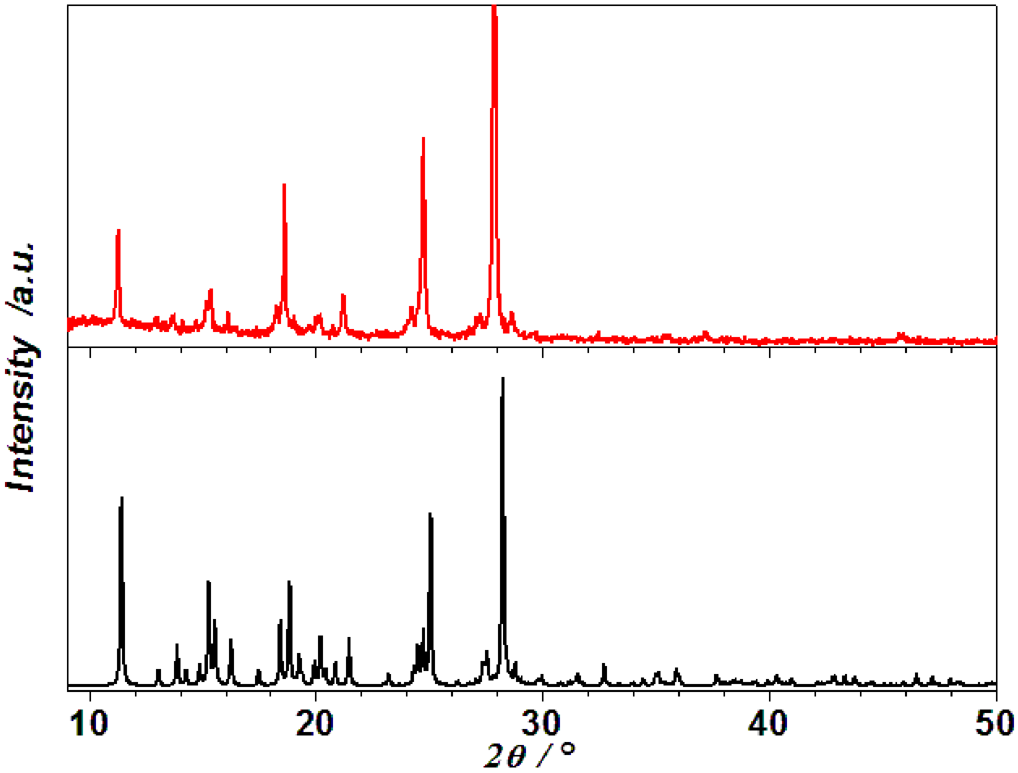

Fig. SI9. The simulative (black line) and experimental (red line) powder X-ray diffraction patterns for H$\mathbf{L}_{\mathbf{2-H}}$.

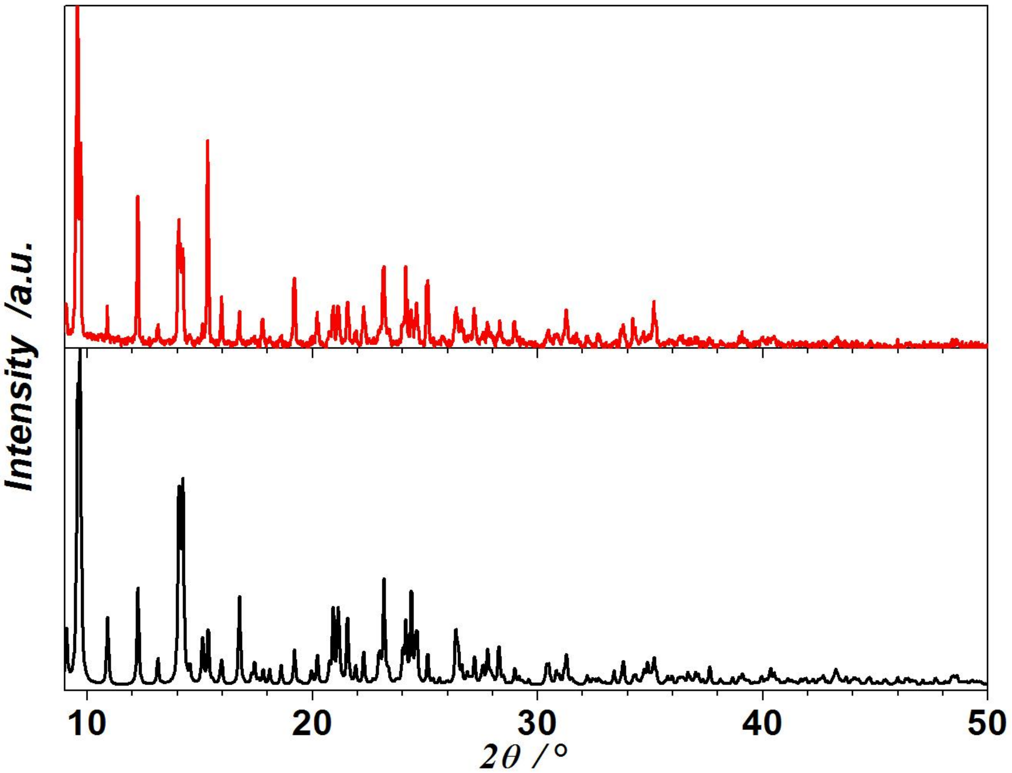

Fig. SI10. The simulative (black line) and experimental (red line) powder X-ray diffraction patterns for $Cu_2(\mathbf{L}_{\mathbf{2\text{-}A}})_4$.

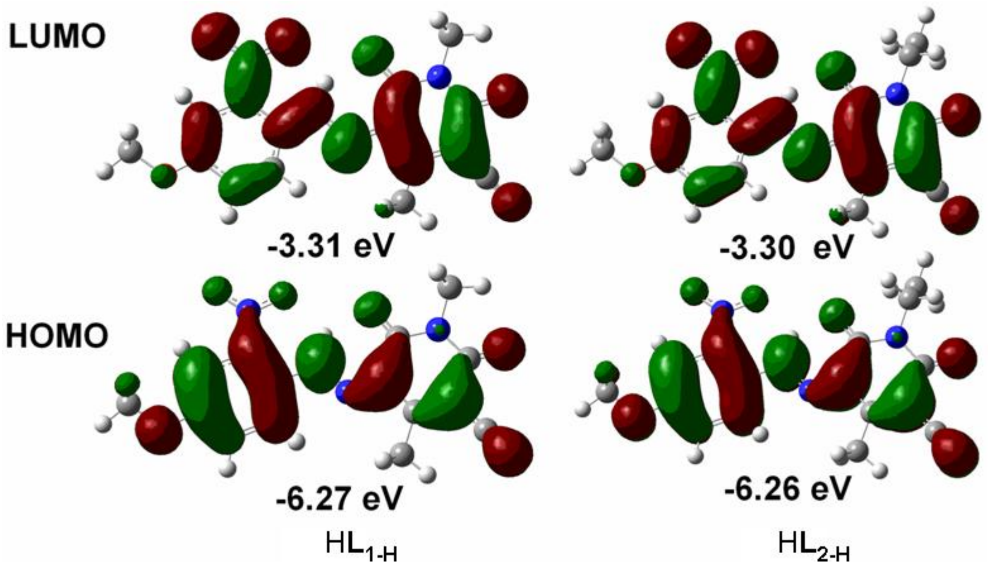

Fig. SI1. Calculated spatial representations of HOMOs and LUMOs for dyes $H\mathbf{L}_{\mathbf{1\text{-}H}}$ and $H\mathbf{L}_{\mathbf{2\text{-}H}}$ with the B3LYP/6–31(d) level.

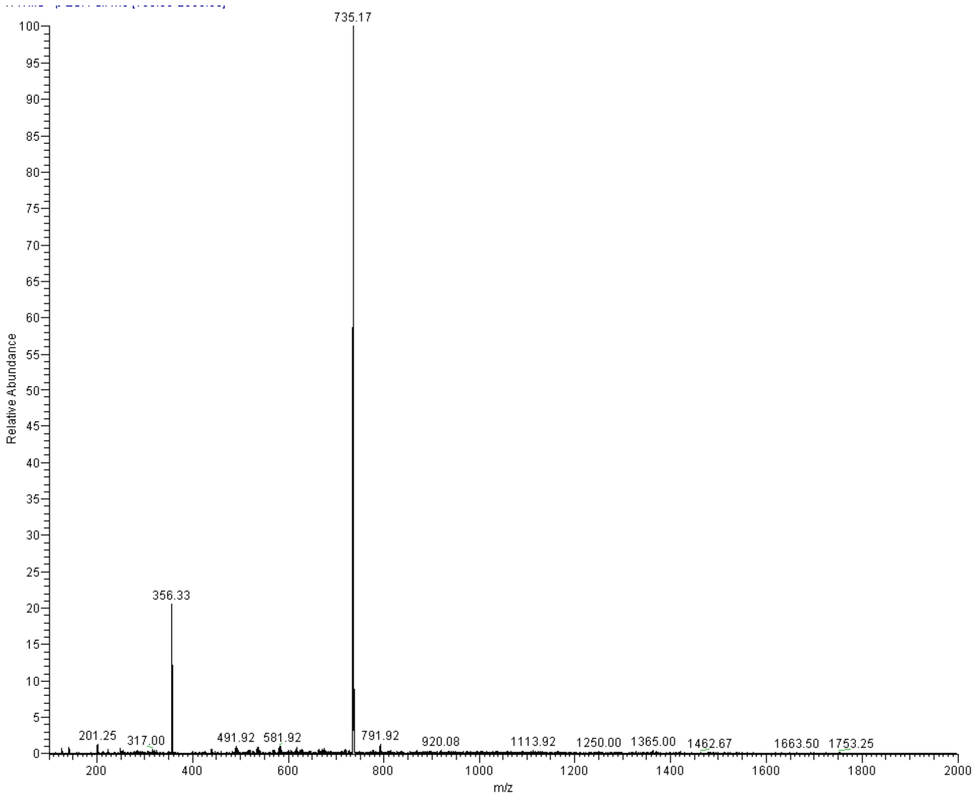

Fig. SI12. ESI–TOF–MS spectrum of $Cu_2(\mathbf{L_{2\text{-}A}})_4$ in the negative ion mode.

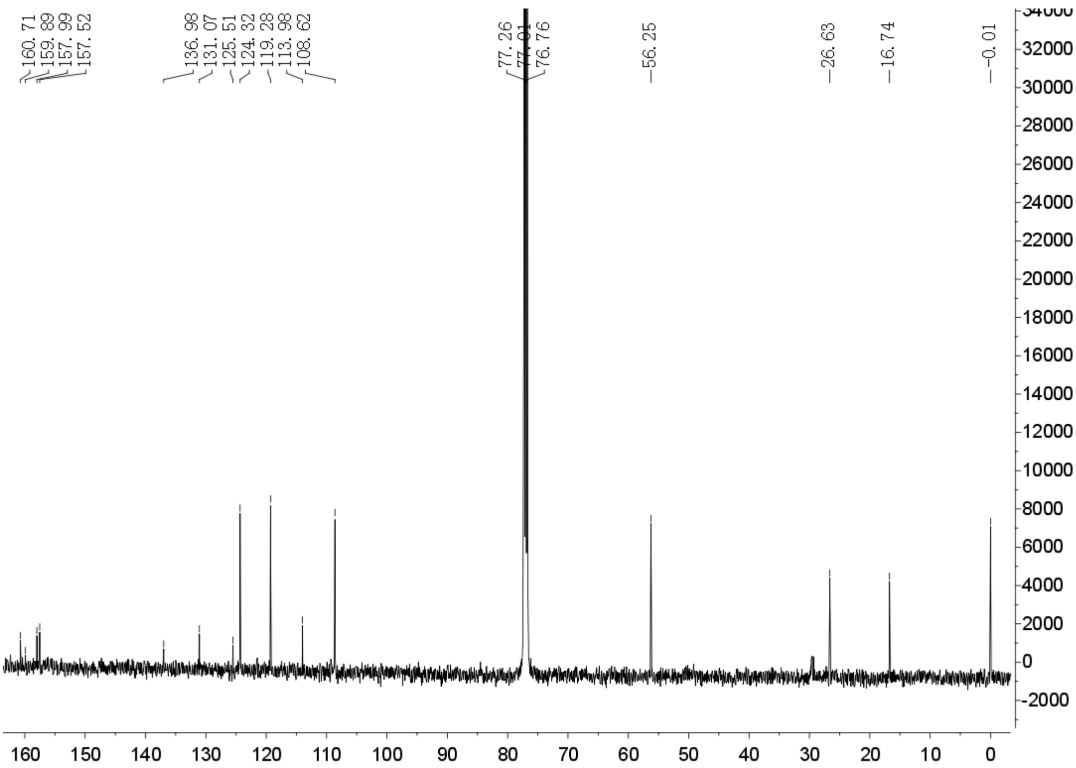

Fig. SI13. ^{13}C NMR spectrum of $H\mathbf{L_{1\text{-}H}}$.

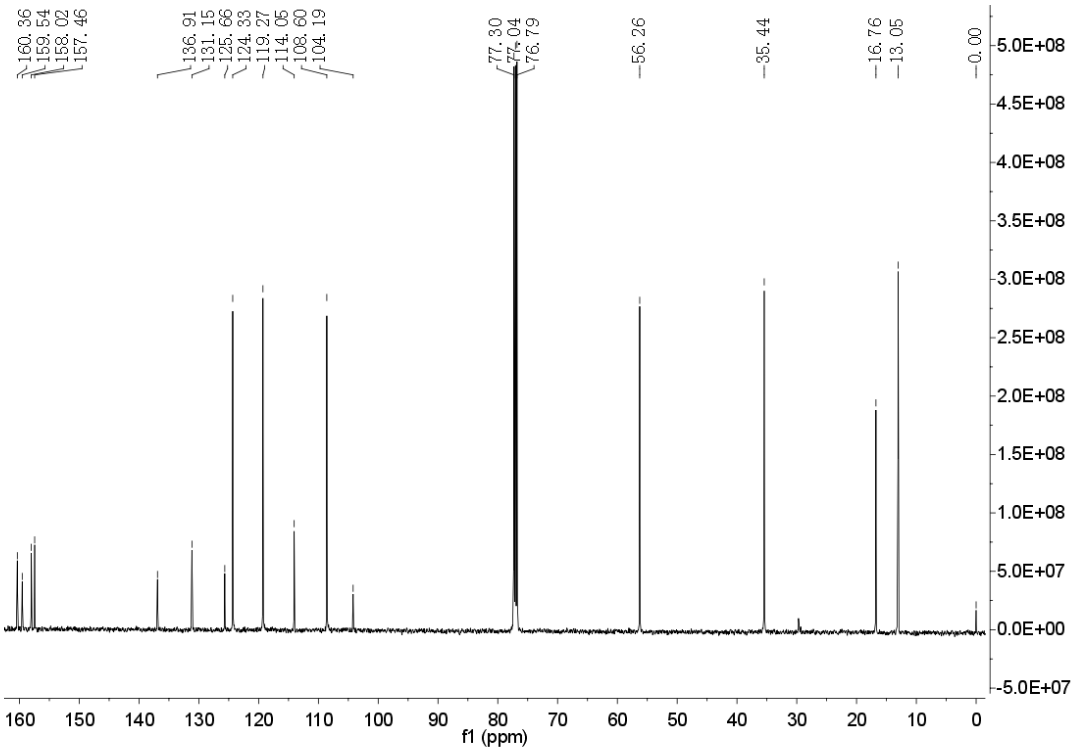

Fig. SI14. ^{13}C NMR spectrum of H$\mathbf{L}_{\mathbf{2\text{-}H}}$.